Damage by radicals and photons during plasma cleaning of porous low-*k* SiOCH. I. Ar/O_2 and He/H_2 plasmas

Juline Shoeb[a)]
Department of Electrical and Computer Engineering, Iowa State University, Ames, Iowa 50011

Ming Mei Wang[b)]
Department of Chemical and Biological Engineering, Iowa State University, Ames, Iowa 50011

Mark J. Kushner[c)]
Department of Electrical Engineering and Computer Science, University of Michigan, Ann Arbor, Michigan 48109

(Received 16 February 2012; accepted 26 April 2012; published 29 May 2012)

Porous dielectric materials offer lower capacitances that reduce *RC* time delays in integrated circuits. Typical porous low dielectric (low-*k*) materials include SiOCH—silicon dioxide with carbon groups, principally $–CH_3$, lining the pores. Fluorocarbon plasmas are often used to etch such low-*k* materials. These processes leave a fluorocarbon polymer on the SiOCH surface that must be removed, often with oxygen or hydrogen containing plasmas. Pores open to the surface and that are internally connected provide pathways for reactive species to enter into the porous network and produce damage. For example, during cleaning using O_2 containing plasmas, reactions of O atoms with $–CH_3$ groups can increase the *k*-value by removing C atoms. Vacuum ultraviolet (VUV) photons produced by the plasma and that penetrate into the material can scission $–Si–CH_3$ bonds and accelerate the removal of $–CH_3$ groups. This paper reports on results from a computational investigation of Ar/O_2 and He/H_2 plasma cleaning of porous SiOCH when including the effects of VUV photons. The authors found that He/H_2 plasmas are able to clean CF_x polymers deposited during etching while producing milder damage to underlying $–CH_3$ sites compared to O_2 plasmas due to the lower reactivity of H atoms and the shorter penetration distance of photons produced in He/H_2 plasmas. © *2012 American Vacuum Society*. [http://dx.doi.org/10.1116/1.4718444]

I. INTRODUCTION

The lower dielectric constant (low-*k*) and lower capacitance of porous materials used for the interlayer dielectric in integrated circuits reduces signal propagation delays. Typical low-*k* materials include porous SiO_2 with methyl groups ($–CH_3$) lining the pores—SiOCH. Such pristine low-*k* materials are essentially hydrophobic (because of the presence of hydrophobic $–CH_3$ groups) and so do not absorb more than a few percent of water when exposed to air even when the humidity is high.[1] This moisture can be driven out of the porous network by heating to 200 °C without detrimentally affecting the stability of the porous material.[2] However, when porous low-*k* SiOCH is exposed to oxygen and hydrogen containing plasmas, $–CH_3$ groups are etched and the nature of the dielectric changes from hydrophobic toward hydrophilic.[1] Free radical –Si• sites produced by plasma exposure can adsorb water from the environment, which then increases the dielectric constant.

Fluorocarbon containing plasmas are often used to etch SiOCH, a process that deposits CF_x polymers on the sidewalls of the features and inside surface lining pores. Although the polymer can effectively seal the surface pores to block moisture uptake,[1] these CF_x polymers are usually removed, as they can cause compatibility issues in subsequent processing steps. For example, halogen containing polymers can react with the diffusion barrier metals Ti and Ta.[3] Also, these polymers can introduce hydrophilic properties since, on a relative basis, they are not as hydrophobic as $–CH_x$ groups.[1] It has been reported that after a fluorocarbon etch, porous SiOCH can adsorb water from the ambient air to volume fractions as high as 8%, which questions the hydrophobicity and sealing efficiency introduced by CF_x polymers.[1]

The removal of the CF_x layer is ideally performed using an oxygen containing plasma due to the efficiency of etching the polymer by oxygen radicals.[4–6] As such, O_2 containing plasmas have often been used for such postetch cleaning and photoresist removal.[7] However, O_2 plasma cleaning can also remove hydrophobic groups from SiOCH (such as removing $–CH_3$ from $–SiO_2–CH_3$), replacing them with hydrophilic groups (such as $–SiO_2–OH$) that can initiate further adsorption of H_2O that increases the dielectric constant.[7–11] $–SiO_2–OH$ accelerates additional water uptake by creating $–SiO_2–OH(H_2O)$ like compounds through hydrogen bonding.[9–11] It has been reported that with the high dielectric constant of water ($k \approx 80$), loss of hydrophobic $–CH_3$ groups and incorporation of water from humid air can increase the dielectric constant *k* from 2.5 to 20 within 10 min of O_2 plasma treatment.[2]

Reducing the hydrophobic nature of SiOCH has a nearly linear relationship with carbon depletion.[1] As a result, a

[a)]Present address: Lam Research, 4400 Cushing Pkwy., Fremont, CA 94538; electronic mail: juline.shoeb@lamrc.com
[b)]Present address: GLOBALFOUNDRIES U.S. Inc., 400 Stonebreak Road Ext., Malta, NY 12020; electronic mail: mingmei.wang@globalfoundries.com
[c)]Author to whom correspondence should be addressed; electronic mail: mjkush@umich.edu

cleaning process that minimizes C depletion will also help to maintain the hydrophobic properties of the film. In this regard, SiOCH is relatively stable when H_2 plasmas are used for cleaning compared to using Ar/O_2 plasmas.[12] (The addition of He to the H_2 plasma aids in preconditioning the surface to improve pore sealing in subsequent treatment using NH_3 containing plasmas.[13–15]) It has also been reported that He/H_2 plasmas are an attractive option for photoresist (PR) mask removal due to there being a small increase of the dielectric constant of SiOCH during the ashing process.[16]

These processes are complicated by the presence of vacuum ultraviolet (VUV) radiation from the plasma coincident to the fluxes of radicals and ions. VUV photons can produce scission of nearly all bonds in the SiOCH films and of the Si–C bond in $–SiO_2–CH_3$ in particular. Such bond scissioning has the potential of accelerating damage by generating sites that react with plasma-produced species at locations that would otherwise be nonreactive with the same species. These sites are likely to react with or hydrogen bond with water, which further increases the dielectric constant.

In this paper, we discuss reaction mechanisms and computationally analyze the damage of porous SiOCH during cleaning with Ar/O_2 and He/H_2 plasmas when considering the consequences of VUV photon fluxes from the plasma. The Hybrid Plasma Equipment Model (HPEM) was used to obtain the ion energy and angle distributions of reactive fluxes from inductively coupled plasmas with capacitive substrate biases for cleaning, and from capacitively coupled plasmas for etching.[17] These distributions were then used as input to the Monte Carlo Feature Profile Model (MCFPM) to predict profiles and composition of the SiOCH.[18] Damage of the porous SiOCH was characterized by the depth at which removal of $–CH_3$ is observed—the demethylation depth. For pores that are not in the line-of-sight to the plasma, diffusion of reactive species into the porous SiOCH is required for damage to occur in the absence of VUV photons. In this regard, we found that deeply penetrating plasma-produced photons can produce Si–C bond scissioning, which accelerates the removal of $–CH_3$ groups. Results will be discussed for the cleaning of pores as a function of treatment time, interconnectivity, and photon fluxes.

In the companion paper, Part II,[19] we address the degradation or increase in dielectric constant resulting from water incorporation into SiOCH from humid air after sustaining damage from plasma cleaning. Removal of $–CH_3$ groups from $–SiO_2–CH_3$ during plasma cleaning produces free radical sites $–SiO_2•$, which react with water vapor to form $–SiO_2–OH$ and $–SiO_2–OH(H_2O)$. Both of these species increase the hydrophilic properties and increase the dielectric constant of the SiOCH.

The reaction mechanisms for plasma damage of SiOCH are discussed in Sec. II, followed by a discussion of plasma properties in Sec. III. Removal of hydrophobic $–CH_3$ and its dependence on interconnectivity, porosity, and photon fluxes are discussed in Sec. IV. Consequences of VUV photon fluxes are discussed in Sec. V and a comparison of our computed trends with prior works is discussed in Sec. VI. Our concluding remarks are in Sec. VII.

II. SURFACE REACTION MECHANISMS

A reaction mechanism was developed for plasmas sustained in He/H_2 and Ar/O_2 mixtures and their interactions with porous SiOCH. The HPEM was employed to obtain the energy and angular distributions for charged and neutral species incident onto the surface.[17] The HPEM has been previously described and so is only briefly summarized here. The HPEM is a two-dimensional, modular model that addresses gas phase and surface kinetics. Electromagnetic fields are derived by solving the frequency domain wave equation based on coil currents adjusted to deliver a specified power deposition. The spatially dependent power deposition is used as a source term in obtaining the electron temperature, T_e, from an electron energy conservation equation. Transport and rate coefficients as function of average electron energy are obtained from a solution of Boltzmann's equation, and a Monte Carlo simulation is used to follow the trajectories of sheath accelerated secondary electrons. The transport coefficients and source functions are used by the fluid kinetics module (FKM) to solve separate continuity, momentum, and energy equations for each ion and neutral species, while semi-implicitly solving Poisson's equation for the time varying electrostatic potential. The densities and electrostatic fields from the FKM are then transferred to the other modules. This process is iterated until a converged quasi-steady-state solution is obtained.

Reaction probabilities for gas phase species with surfaces are provided by the surface chemistry module (SCM), which computes the composition of surface resident species using a multilayer surface-site-balance model. The reaction mechanism is unique for each surface in contact with the plasma. The Plasma Chemistry Monte Carlo Module (PCMCM) produces the energy and angular distributions for neutrals and ions striking surfaces in contact with the plasma. The PCMCM launches pseudoparticles representing ions and neutrals based on the electron impact source functions. Using time dependent electric fields from the FKM, their trajectories are integrated while accounting for gas phase collisions. The energy and angular distributions (EADs) of neutral and ion pseudoparticles are recorded as they strike surfaces.

The SCM and MCFPM incorporate energy dependent reaction probabilities based on the EADs obtained from the PCMCM. The probabilities for surface reactions involving energetic species (either ions or hot neutrals) are given by[17]

$$p(E) = p_0 \frac{E^m - E_t^m}{E_r^m - E_t^m}, \tag{1}$$

where $p(E)$ is the reaction probability for a particle with energy E, E_t is the threshold energy of the process, E_r is a reference energy, and p_0 is the reaction probability at the reference energy. We used $m = 0.5$ in this work.

The Monte Carlo Radiation Transport Module (MCRTM) in the HPEM is called after each iteration to provide photon fluxes incident onto the SiOCH.[18] The operation of MCRTM is similar to the operation of PCMCM. Source functions for launching of pseudoparticles representing photons are

derived from the excited state densities generated by the FKM. The trajectory of a photon is tracked until it is absorbed by a gas phase species or it strikes a surface. The photon absorption probability is obtained from a Voight line shape function using the natural lifetime, collisional broadening, and Doppler broadening produced by the local gas densities and temperatures. If resonantly absorbed, photons are re-emitted using a partial-frequency redistribution algorithm. The fluxes and spectra of photons are recorded as a function of the material the photons strike, and are exported to the surface kinetics module SCM and the MCFPM. The rates of photon absorption and re-emission are recorded for each optical transition, and are used to calculate radiation trapping factors, which lengthen the natural lifetime of the emitting species. These factors are exported to the FKM.

The damage mechanism for SiOCH to be discussed in the following was implemented in the MCFPM with which the evolution of the SiOCH and damage are predicted.[20] The MCFPM resolves the porous material with approximately atomic resolution. The numerical cell size in this work is $0.4\,\text{nm} \times 0.4\,\text{nm}$, which is an effective radius of 0.2 nm. The creation of pores in the MCFPM mesh is discussed in Ref. 21. The internal surfaces of the pores in SiO_2 were lined with a single layer of $–CH_3$ to approximate the structure of SiOCH.

Using the angular distribution of fluxes provided by the MCRTM, the MCFPM then addresses photon penetration into the SiOCH. In principle, the MCFPM treats photons similarly to radicals or ions. Based on the magnitude and angular distribution of photons of different wavelengths, a pseudoparticle representing a photon is randomly directed toward the substrate. For each material in the mechanism an absorption length is specified. The probability that a photon m will be absorbed by material j crossing cell i is $p_{imj} = 1 - \exp(\lambda_{mj}\ell_i)$, where λ_{mj} is the absorption length in material j for photon m and ℓ_i is the traversal distance of the photon across the cell i. When a photon enters into a material cell, this probability is evaluated. If $r \le p_{imj}$, where r is a random number distributed on (0, 1), the photon is absorbed. Otherwise, the photon continues along its trajectory. When absorbed, the material identity of the solid cell is changed based on the reaction mechanism.

For the Ar/O_2 plasmas of interest, the UV and VUV fluxes are dominated by emission from oxygen species.[22] Electron impact excitation of O atoms generates O($3s$), O($5s$), and O($5p$) states. The O($3s$) emits 130 nm photons and O($5s$) emits 136 nm photons in relaxing to ground state. O($5p$) also emits 777 nm photons in relaxing to O($5s$). To simplify the reaction mechanism in the MCFPM we considered only radiation transport into solid materials of the 130 nm photons. The penetration distance of 130 nm photons into porous SiOCH is $\lambda \approx 100\,\text{nm}$.[23–25] In low pressure He/H_2 plasmas, damaging VUV fluxes are dominated by resonance radiation from He($2\,^1p$) at 58.4 nm having a penetration depth of ≈20 nm in the porous SiOCH.[13,24] The damage mechanisms of these VUV photons are dominantly bond breaking. For example, the 130 and 58.4 nm photons have enough energy to break both Si–C and Si–O bonds. In the former case, the dissociated $\bullet CH_3$ remains physisorbed or trapped. In the latter case, the Si–O is converted to a free radical site (denoted as SiO_2^* here).

It is believed that reactions of O radicals with CH_3 groups of SiOCH are the primary mechanism for C depletion during Ar/O_2 plasma processing SiOCH films.[8,26] With interconnected porous SiOCH, oxygen atoms can diffuse into the porous network and react with the hydrophobic $–CH_3$ groups in $–SiO_2–CH_3$ located on the pore-walls well below the surface.[27] The carbon in the $–CH_3$ groups is likely removed as CO or CO_2.[27–29] Reactions of O atoms can also abstract H from $–SiO_2–CH_3$ leaving $–SiO_2–CH_2\bullet$.[27] O radicals having an energy >0.1 eV can break the Si–C bond of $–SiO_2–CH_n$ that eventually leads to the formation of CO and H_2O leaving behind a free radical Si• site on the surface of the pore.[26,27] Si–C bond scission in $–SiO_2–CH_3$ by VUV photons leaves behind trapped $\bullet CH_3$, which can be later etched by O atoms.[23,25,26] By trapped, we refer to a low mobility surface state of $\bullet CH_3$. We note that O_2 plasmas do not significantly etch SiO_2, and so their primary reactions are with the carbon contained in CH_3 groups.[28]

The probabilities in the following reactions for both surface site modification and $–CH_3$ etching in Ar/O_2 and He/H_2 plasmas have been determined by extensive parameterization of the models to be qualitatively consistent with experimental results available in the literature. Bounds of reaction probabilities are set based on thermodynamic properties and the change in enthalpy of reactions. Within those bounds, parameterization and comparison to experiments refines the mechanism. Examples of works that guided the development of the reactions are discussed in Sec. VI.

The reactions for removal of $–CH_3$, or demethylation of SiOCH, in plasmas containing O_2 are listed in Table. I.[23,25–29] In these mechanisms, the subscript g denotes a gas phase species, subscript a denotes an adsorbed or trapped species, the number of closed circles (•) represents the number of dangling bonds on the free radical site, and dashes (–) represents bonding to the solid. (A complete reaction mechanism consisting of many hundreds of reactions can be obtained by request from the authors.)

Oxygen radicals, O, can directly and exothermically react with $–SiO_2–CH_3$ through H abstraction to form OH and a free radical site. O atoms with energy >0.1 eV can produce Si–C bond scission as suggested in Ref. 26, in turn producing $\bullet CH_{3a}$. Both of these outcomes are vulnerable to further O radical or O_2 attack that eventually removes methyl groups. To etch $–CH_3$ groups in Ar/O_2 plasmas, Si–C bond breaking caused by VUV photons is not essential. However, if photons are present, Si–C bond scission occurs, which can accelerate removal of $–CH_3$ groups. Etch products of such $–CH_3$ removal reactions include CO, CO_2, and H_2O. Such internally generated H_2O during $–CH_3$ etching can react with $–SiO_2\bullet$ sites forming $–SiO_2–OH$, which can contribute to an increase in the dielectric constant.

He/H_2 plasmas remove $–CH_3$ groups from SiOCH at a slower rate compared to O_2 containing plasmas primarily due to the higher threshold energies for these reactions involving H atoms. In addition, the reactions responsible for $–CH_3$

TABLE I. Reaction mechanisms for porous SiOCH damage in Ar/O_2 plasmas.

Species	
M_g	Gas phase species
M	Surface site
–M	Surface site bonded to a solid
M•	Active surface site with dangling bond
M_a	Adsorbed or trapped surface site
M_g^+	Ion

No.	Reaction[a–c]	Probability
1	$O_g + -SiO_2-CH_3 \rightarrow -SiO_2-CH_2\bullet + OH_g$,	0.005[d]
2	$O_g + -SiO_2-CH_3 \rightarrow -SiO_2\bullet + \bullet CH_{3a} + O_g$	0.005[d]
3	$OH_g + -SiO_2-CH_3 \rightarrow -SiO_2-CH_2\bullet + H_2O_g$	0.004[d]
4	$h\nu(130\text{nm}) + -SiO_2-CH_3 \rightarrow -SiO_2\bullet + \bullet CH_{3a}$	0.800
5	$O_g + -SiO_2-CH_2 \rightarrow -SiO_2\bullet + CH_2O\bullet_a$	0.004
6	$O_g + \bullet CH_{3a} \rightarrow CH_2O\bullet_a + H_g$	0.004
7	$O_g + CH_2O\bullet_a \rightarrow CO_g + H_2O_g$	0.004
8	$O_{2g} + \bullet CH_{3a} \rightarrow CH_2O\bullet_a + OH_g$	0.004
9	$O_{2g} + CH_2O\bullet_a \rightarrow CO_g + H_2O_g$	0.004
10	$H_2O_g + -SiO_2\bullet \rightarrow -SiO_2-OH + H_g$	1.5×10^{-5}
11	$O_g^+ + -SiO_2-CH_3 \rightarrow -SiO_2\bullet + CH_{3g} + O_g$	10^{-4} [e]
12	$O_g^+ + -SiO_2-CH_3 - SiO_2\bullet + -CH_2\bullet + OH_g$	10^{-4} [e]
13	$O_g^+ + -SiO_2-CH_2\bullet \rightarrow -SiO_2\bullet + CH_{2g} + O_g$	10^{-4} [e]
14	$O_g^+ + -SiO_2-CH_2\bullet \rightarrow -SiO_2\bullet + -CH\bullet\bullet + OH_g$	10^{-4} [e]
15	$O_{2g}^+ + -SiO_2-CH_3 \rightarrow -SiO_2\bullet + CH_{3g} + O_{2g}$	10^{-4} [e]
16	$O_{2g}^+ + -SiO_2-CH_3 \rightarrow -SiO_2\bullet + CH_2O\bullet_a + OH_g$	10^{-4} [e]
17	$O_{2g}^+ + -SiO_2-CH_2\bullet \rightarrow -SiO_2\bullet + CH_{2g} + O_{2g}$	10^{-4} [e]
18	$O_{2g}^+ + -SiO_2-CH_2\bullet \rightarrow -SiO_2\bullet + CH_2O\bullet_a + O_g$	10^{-4} [e]
19	$O_g^+ + \bullet CH_{3a} \rightarrow CH_{3g} + O_g$	10^{-4} [e]
20	$O_{2g}^+ + \bullet CH_{3a} \rightarrow CH_{3g} + O_{2g}$	10^{-4} [e]

[a]Unless specified, all ions neutralize on surfaces, returning as their neutral counterparts. A preceding dash denoted bonding to the solid.
[b]Gas phase species have units of flux ($cm^{-2}\ s^{-1}$). Surface species have units of fractional coverage.
[c]In reactions with no chemical change, the gas species are reflected off the surface. These reactions are not shown.
[d]$E_r = 3.5$ eV, $E_t = 0.18$ eV, probability is at E_r.
[e]$E_r = 100$ eV, $E_t = 10$ eV, probability is at E_r.

removal in He/H_2 plasmas likely produce less volatile products, such as CH_4, which are less likely to continue reacting with the SiOCH. In other contexts, He plasma pretreatment of SiOCH has been found to produce surface modifications that can minimize further damage.[13–15] He^+ and photons from He/H_2 plasmas can remove H from $–SiO_2–CH_3$ producing $–SiO_2–CH_n$ ($n = 0, 1, 2$) that have lower etch rates. This is because H is only efficient in removing C from $–SiO_2–CH_3$ among all $–SiO_2–CH_n$ ($n = 0$–3) products as volatile CH_4. Since the activation energy to remove C from $–SiO_2–CH_3$ increases as n decreases, the rate of C removal from $–SiO_2–CH_n$ by thermal H atoms decreases as H is removed. Although hot H atoms (H*) are able to produce this etching, H* typically have above threshold energies only near the surface. By the time H atoms diffuse into the pores, their energy has largely been thermalized to below the threshold energies required to etch $–SiO_2–CH_n$ ($n < 3$). To etch these compounds, they would first need to be saturated back to $–SiO_2–CH_3$ through H adsorption, followed by H atom etching $–CH_3$ as volatile CH_4. The end result is that generation of $–SiO_2–CH_n$ ($n < 3$) by photons or ions could slow $–CH_3$ removal.

In certain parameter spaces of operating of low pressure He/H_2 plasmas, it is possible to produce significant fluxes of hot H atom (H*) fluxes to the substrate through dissociative excitation, charge exchange, and vibrational-translational (VT) reactions. Hot H atom generation mechanisms are discussed in Sec. III.

Hot H atoms in this context have translational energies of up to or exceeding a few tenths of an eV. H atoms with energies >0.4 eV are able to abstract H from $–SiO_2–CH_3$ producing $–SiO_2–CH_n$ ($n = 1$, 2), which slows the rate of carbon removal. Cleaving of Si–C bonds by photons produces trapped $\bullet CH_{3a}$ groups that can be later etched by an H atom as CH_4.[13,14,29] After $–CH_3$ removal from $–SiO_2–CH_3$, H atoms can passivate the resulting $–SiO_2\bullet$ site by forming $–SiO_2–H$, which is hydrophobic in nature and can also block subsequent water update.[30] However, He^+ can also break the Si–O bond in $–SiO_2\bullet$ and generate the free radical site $–SiO\bullet\bullet$, and a subsequent collision can produce $–Si\bullet\bullet\bullet$, though the frequency of occurrence of these sites is low. H can passivate $–Si\bullet\bullet\bullet$ forming $–Si–H_n$ ($n = 1$–3). Such Si–H bond compounds are also hydrophobic in nature and can block water uptake. As such, even after the $–CH_3$ group removal, He/H_2 plasma treatment may be able to maintain some hydrophobic properties of the SiOCH.

Reactions during He/H_2 plasma treatment of SiCOH are listed in Table II.[13,14,25,29,30] Among these reactions, H reactions that involve removal of $–CH_3$ groups or demethylation (reactions 6 and 13) and abstraction of H from $–CH_n$ ($n = 1$–3) (reactions 15–35) are endothermic, and require hot H atoms or vibrationally excited H_2 to quickly proceed. However, $–CH_3$ removal reactions are less endothermic than H abstraction reactions and H passivation of $–SiO_2–CH_n$. $–Si\bullet\bullet\bullet$, and $–Si–H_n$ ($n = 1$, 2, 3). Reactions 10 and 11 are exothermic in nature.

PR that is dominantly a hydrocarbon can be removed by O atoms from Ar/O_2 plasmas by forming compounds such as CHO, while hot H atoms (>0.5–1 eV) and vibrationally excited H_2 ($v > 2$) produced in He/H_2 plasmas can remove PR by forming compounds such as CH_4. O containing ions such as O^+ and O_2^+ can etch PR either physically or chemically. H containing ions H^+, H_2^+, and H_3^+ chemically etch PR as CH_4. Energetic ions such as Ar^+ and He^+ can physically sputter PR. The mechanism for removal of PR in Ar/O_2 and He/H_2 plasmas is listed in Table III. PR etching reactions that involve O species (reactions 1–3) are exothermic. H atom or H_2 ($v > 3$) etching reactions (reactions 4–10) are endothermic. SiO_2^* (bond cleaved SiO_2) which is generated by VUV photons is not believed to be chemically active in H_2 or O_2 plasmas. It has been reported that SiO_2^* can only adsorb O in Ar/O_2 plasmas forming an SiO_2-like layer (without showing any etching of SiO_2).[29] Similarly, H is adsorbed by SiO_2^* without causing any Si consumption in He/H_2 plasmas. Given these trends, and since the emphasis of this study is on demethylation, we excluded SiO_2^* reactions in Ar/O_2 or He/H_2 plasmas for simplicity.[29,31]

TABLE II. Reaction mechanism for porous SiOCH damage in He/H_2 plasmas.

Species		
M_g	Gas phase species	
M	Surface site	
–M	Surface site bonded to a solid	
M•	Active surface site with dangling bonds	
M_a	Adsorbed or trapped surface site	
M_g^+	Ion	
No.	Reaction[a–c]	Probability
1	$h\nu(\approx 58\,\text{nm}) + -SiO_2–CH_3 \rightarrow -SiO_2\bullet + \bullet CH_{3a}$	0.9
2	$He_g^+ + -SiO_2–CH_3 \rightarrow -SiO_2–CH_2\bullet + H_g + He_g$	0.4[d]
3	$He_g^+ + -SiO_2–CH_2\bullet \rightarrow -SiO_2–CH\bullet\bullet + H_g + He_g$	0.4[d]
4	$He_g^+ + -SiO_2–CH\bullet\bullet \rightarrow -SiO_2–C\bullet\bullet\bullet + H_g + He_g$	0.4[d]
5	$He_g^+ + -SiO_2\bullet \rightarrow -SiO\bullet\bullet + -O\bullet + He_g$	0.4[d]
6	$He_g^+ + -SiO\bullet\bullet \rightarrow -Si\bullet\bullet\bullet + -O\bullet + He_g$	0.4[d]
7	$H_g + -SiO_2–CH_3 \rightarrow -SiO_2\bullet + CH_{4g}$	10^{-5}[e]
8	$H_g + -SiO_2–C\bullet\bullet\bullet \rightarrow -SiO_2–CH\bullet\bullet$	10^{-5}
9	$H_g + -SiO_2–CH\bullet\bullet \rightarrow -SiO_2–CH_2\bullet$	10^{-5}[e]
10	$H_g + -SiO_2–CH_2\bullet \rightarrow -SiO_2–CH_3$	10^{-5}[e]
11	$H_g + -SiO_n\bullet \rightarrow -SiO_n–H$	0.1
12	$H_g + -Si\bullet\bullet\bullet \rightarrow -Si–H\bullet\bullet$	0.01
13	$H_g + -Si–H_x\bullet \rightarrow -Si–H_{x+1}$	0.001
14	$H_g + \bullet CH_{3a} \rightarrow CH_{4g}$	0.03[f]
15	$H_g + -O\bullet \rightarrow -OH$	0.01
16	$H_g + -SiO_2–CH_3 \rightarrow -SiO_2–CH_2\bullet + H_{2g}$	0.75[g]
17	$H_g + -SiO_2–CH_2\bullet \rightarrow -SiO_2–CH\bullet\bullet + H_{2g}$	0.75[g]
18	$H_g + -SiO_2–CH\bullet \rightarrow -SiO_2–C\bullet\bullet + H_{2g}$	0.75[g]
19	$H_2(v=0)_g + -SiO_2–CH_3 \rightarrow -SiO_2–CH_2\bullet + H_{2g}$	0.75[h]
20	$H_2(v=0)_g + -SiO_2–CH_2\bullet \rightarrow -SiO_2–CH\bullet\bullet + H_{2g}$	0.75[h]
21	$H_2(v=0)_g + -SiO_2–CH\bullet\bullet \rightarrow -SiO_2–C\bullet\bullet\bullet + H_{2g}$	0.75[h]
22	$H_2(v=0)_g + -SiO_2–CH_3 \rightarrow -SiO_2–CH_2\bullet + H_{2g}$	0.75[h]
23	$H_2(v=1)_g + -SiO_2–CH_2\bullet \rightarrow -SiO_2–CH\bullet\bullet + H_{2g}$	0.75[h]
24	$H_2(v=1)_g + -SiO_2–CH\bullet\bullet \rightarrow -SiO_2–C\bullet\bullet\bullet + H_{2g}$	0.75[h]
25	$H_2(v=2)_g + -SiO_2–CH_3 \rightarrow -SiO_2–CH_2\bullet + H_{2g}$	0.75[h]
26	$H_2(v=2)_g + -SiO_2–CH_2\bullet \rightarrow -SiO_2–CH\bullet\bullet + H_{2g}$	0.75[h]
27	$H_2(v=2)_g + -SiO_2–CH\bullet\bullet \rightarrow -SiO_2–C\bullet\bullet\bullet + H_{2g}$	0.75[h]
28	$H_2(v=3)_g + -SiO_2–CH_3 \rightarrow -SiO_2–CH_2\bullet + H_{2g}$	0.75[h]
29	$H_2(v=3)_g + -SiO_2–CH_2\bullet \rightarrow -SiO_2–CH\bullet\bullet + H_{2g}$	0.75[h]
30	$H_2(v=3)_g + -SiO_2–CH\bullet\bullet \rightarrow -SiO_2–C\bullet\bullet + H_{2g}$	0.75[h]
31	$H_2(v=4)_g + -SiO_2–CH_3 \rightarrow -SiO_2–CH_2\bullet + H_{2g}$	0.75[h]
32	$H_2(v=4)_g + -SiO_2–CH_2\bullet \rightarrow -SiO_2–CH\bullet\bullet + H_{2g}$	0.75[h]
33	$H_2(v=4)_g + -SiO_2–CH\bullet\bullet \rightarrow -SiO_2–C\bullet\bullet\bullet + H_{2g}$	0.75[h]
34	$H_2(v=5)_g + -SiO_2–CH_3 \rightarrow -SiO_2–CH_2\bullet + H_{2g}$	0.75[h]
35	$H_2(v=5)_g + -SiO_2–CH_2\bullet \rightarrow -SiO_2–CH\bullet\bullet + H_{2g}$	0.75[h]
36	$H_2(v=5)_g + -SiO_2–CH\bullet \rightarrow -SiO_2–C\bullet\bullet\bullet + H_{2g}$	0.75[h]

[a]Unless specified, all ions neutralize on surfaces, returning as their neutral counterparts. A preceding dash denotes bonding to the solid.
[b]Gas phase species have units of flux ($cm^{-2}\,s^{-1}$). Surface species have units of fractional coverage.
[c]In reactions with no chemical change, the gas species are reflected off the surface. These reactions are not shown.
[d]$E_r = 100.0\,\text{eV}$, $E_t = 10.0\,\text{eV}$, probability is at E_r.
[e]$E_r = 3.5\,\text{eV}$, $E_t = 0.5\,\text{eV}$, probability is at E_r.
[f]$E_r = 3.5\,\text{eV}$, $E_t = 0.03\,\text{eV}$, probability is at E_r.
[g]$E_r = 3.5\,\text{eV}$, $E_t = 1.0\,\text{eV}$, probability is at E_r.
[h]$E_r = 3.5\,\text{eV}$, $E_t = 0.3\,\text{eV}$, probability is at E_r.

III. PLASMA PROPERTIES

For purposes of this investigation, plasma cleaning processes were modeled as performed in inductively coupled plasmas (ICPs). The test reactor treated a wafer 15 cm in diameter. The reactor was 26 cm in diameter with a wafer-to-coil height of 10 cm [see Fig. 1(a)]. The conditions for both Ar/O_2 and He/H_2 plasma treatment were 10 mTorr with a flow rate of 100 sccm, where sccm denotes cubic centimeters per minute at standard temperature and pressure. For the

TABLE III. Reaction mechanism for PR removal in Ar/O_2 and He/H_2 plasmas.

Species		
M_g	Gas phase species	
M	Surface site	
M_g^+	Ion	
No.	Reaction[a–c]	Probability
1	$O_g + PR \rightarrow CHO_g$	0.002
2	$O_g^+ + PR \rightarrow CHO_g$	0.002
3	$O_{2g}^+ + PR \rightarrow CHO_g$	0.002
4	$H_g + PR \rightarrow CH_{4g}$	0.010[d]
5	$H_g^+ + PR \rightarrow CH_{4g}$	0.010[d]
6	$H_{2g}^+ + PR \rightarrow CH_{4g}$	0.010[d]
7	$H_{3g}^+ + PR \rightarrow CH_{4g}$,	0.010[d]
8	$H_{2(v=3)g} + PR \rightarrow CH_{4g}$	0.010[d]
9	$H_{2(v=4)g} + PR \rightarrow CH_{4g}$	0.010[d]
10	$H_{2(v=5)g} + PR \rightarrow CH_{4g}$	0.010[d]
11	$He_g^+ + PR \rightarrow PR_g + He_g$	10^{-5} [e]
12	$Ar_g^+ + PR \rightarrow PR_g + Ar_g$	10^{-5} [e]

[a]Unless specified, all ions neutralize on surfaces, returning as their neutral counterparts.
[b]Gas phase species have units of flux ($cm^{-2}\,s^{-1}$). Surface species have units of fractional coverage.
[c]In reactions with no chemical change, the gas species are reflected off the surface. These reactions are not shown.
[d]$E_r = 100$ eV, $E_t = 1.4$ eV, probability is at E_r.
[e]$E_r = 100$ eV, $E_t = 10$ eV, probability is at E_r.

base case, the coil delivered 300 W at 10 MHz. The gas mixtures were $He/H_2 = 75/25$ and $Ar/O_2 = 5/95$. The substrate was biased at 10 MHz.

Typical plasma properties for a power of 300 W are shown in Fig. 1 and reactive fluxes to the substrate are shown in Fig. 2. For Ar/O_2 plasmas, the peak O-atom density is $9.5 \times 10^{13}\,cm^{-3}$ and the peak total ion density is $6 \times 10^{11}\,cm^{-3}$. With a 20 V substrate bias, ions have an average energy near 30 eV and a total flux of $2.3 \times 10^{16}\,cm^{-2}\,s^{-1}$ at the center of the wafer. The individual fluxes include $1.5 \times 10^{16}\,cm^{-2}\,s^{-1}$ for O^+, $0.6 \times 10^{16}\,cm^{-2}\,s^{-1}$ for O_2^+, and $2.1 \times 10^{15}\,cm^{-2}\,s^{-1}$ for Ar^+. O atoms, the dominant agent for $-CH_3$ removal, have a flux of $1.5 \times 10^{18}\,cm^{-2}\,s^{-1}$. The flux of VUV photons is $2.5 \times 10^{13}\,cm^{-2}\,s^{-1}$.

In He/H_2 plasmas, the peak ion density is $3.5 \times 10^{10}\,cm^{-3}$, while H atoms have a maximum density of $1.8 \times 10^{13}\,cm^{-3}$. The ion fluxes ($1.8 \times 10^{16}\,cm^{-2}\,s^{-1}$) largely responsible for the PR removal had an average energy near 30 eV for a 20 V bias and an angular spread from the vertical of $<15°$. The individual fluxes include $4 \times 10^{15}\,cm^{-2}\,s^{-1}$ for H^+, $7 \times 10^{15}\,cm^{-2}\,s^{-1}$ for H_2^+, $1 \times 10^{15}\,cm^{-2}\,s^{-1}$ for H_3^+, and $6 \times 10^{15}\,cm^{-2}\,s^{-1}$ for He^+. The VUV flux is $6 \times 10^{14}\,cm^{-2}\,s^{-1}$ and that for H atoms is $1 \times 10^{18}\,cm^{-2}\,s^{-1}$.

Hot H atoms (H*) have temperatures (or energies) that exceed that of the average gas temperature. The EADs of H atoms incident onto the wafer are shown in Fig. 3 for He/H_2 mixtures for pressures of 10–80 mTorr. H* fluxes to the wafer are also shown as a function of pressure. The EADs are dominated by a thermal isotropic component corresponding

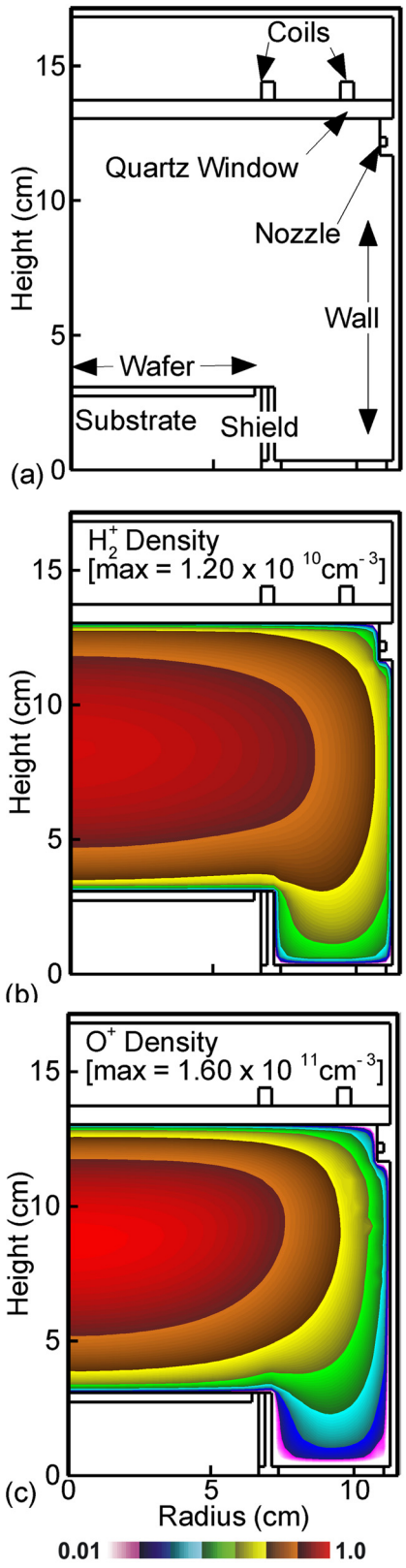

FIG. 1. (Color online) Properties of the inductively coupled plasma cleaning reactors. (a) Schematic of the reactor. Properties of $He/H_2 = 75/25$ plasmas showing (b) the dominant ion H_2^+ (maximum $1.2 \times 10^{10}\,cm^{-3}$). Properties of $Ar/O_2 = 5/95$ plasmas showing (c) the dominant ion O^+ density (maximum $1.60 \times 10^{11}\,cm^{-3}$). Plasma conditions are 300 W ICP, 10 mTorr, 100 sccm.

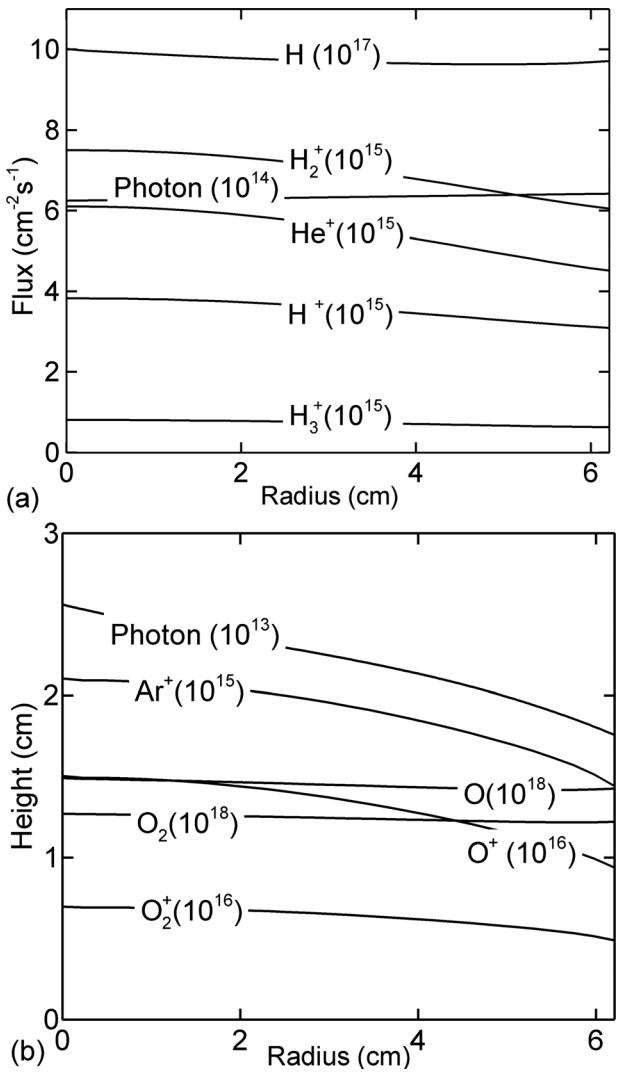

FIG. 2. Ion, photon, and neutral fluxes as a function of radius for (a) He/H_2 and (b) Ar/O_2 plasmas. The scaling for fluxes is indicated. ($He/H_2 = 75/25$, 300 W ICP, 10 mTorr, 100 sccm; $Ar/O_2 = 05/95$, 300 W ICP, 10 mTorr, 100 sccm).

to the gas temperature of ≈800 K. At lower pressures, a significant population of H* is produced, in general also having an isotropic angular distribution. As the pressure increases, the fraction of H* decreases; however, its angular distribution narrows.

The dominant H* generation mechanism is by Frank-Condon heating through the dissociation excitation of $H_2(v \geq 2)$ by electron impact.[32] Although such reactions cannot generate H atoms with energies >4 eV, the energy is sufficient to initiate endothermic polymer cleaning or PR removal reactions. Charge exchange reactions between $H_2(v)$ and H^+, or H^+ and H can generate H atoms with energies as high as the energy of H^+ ions in the plasma. Charge exchange reactions can also occur between $H_2(v)$ and H_2^+ producing translationally hot $H_2(v)$ having sufficient energies to initiate endothermic polymer cleaning or PR etching reactions. As the rate of charge exchange is small compared to dissociative excitation, a small fraction of H* is produced in this manner. H* can also be produced through VT

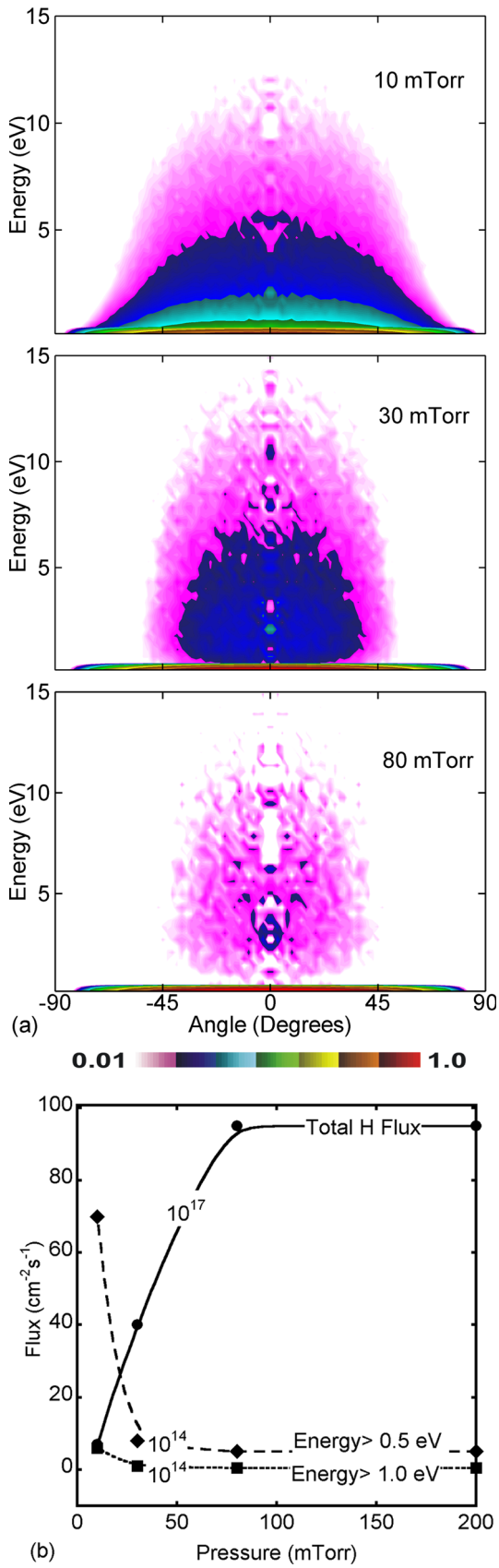

FIG. 3. (Color online) Optimization of hot H (>0.5 eV) fluxes to the wafer by varying pressure ($He/H_2 = 75/25$, 300 W ICP, 100 sccm). (a) Energy and angular distribution of H atoms for pressures of 10, 30, and 80 mTorr. (b) Total H flux, and hot H flux (>0.5 and >1.0 eV) as a function of pressure. The scaling for fluxes is indicated.

reactions of H atoms with $H_2(v)$.[33] In these collisions, $H_2(v)$ molecules are quenched to a state $H_2(v' < v)$, and the H atoms carry away the energy difference as translational energy, 0.5 eV per vibrational level. These VT reactions can give H atoms enough energy to broach the endothermic barrier to clean CF_x polymer or PR.

Optimizing the collisionality of He/H_2 plasmas by changing pressure enables a high rate of H* production while also allowing these H* to reach the wafer. The total H atom flux, and fluxes of H atoms with energies >0.5 and >1 eV as a function of pressure are shown in Fig. 3(b). For pressures >20 mTorr the H* fluxes decrease in large part due to thermalization of initially produced H* before those atoms reach the surface. With an increase in pressure from 10 to 200 mTorr, total H flux rises from 10^{18} to 10^{19} cm^{-2} s^{-1}, while the energy of H atoms decreases. At 10 mTorr, roughly 1% of the H atoms have energies >0.5 eV, which is above the threshold energy to etch PR and remove CF_x polymers. At 30 mTorr, only 0.1% of H atoms have energies >0.5 eV. At pressures of >80 mTorr, the fraction of H atoms with energy >0.5 eV is only 0.006%. Since H* fluxes are required to efficiently remove the CF_x polymer that remains on trench sidewalls after fluorocarbon plasma etching, operating at pressures of less than tens of mTorr is optimum.

IV. DEMETHYLATION

For the base case the pore size is 0.8 nm in diameter (10% standard deviation) with a porosity of 30% and interconnectivity of 100%. $–CH_3$ groups initially line the pore-walls. The calculated dielectric constant is approximately $k = 2.5$, based on the volume fraction of each component of the porous film ($–CH_3$, SiO_2, and air gap) and their individual dielectric constants.[34]

Trenches were etched into SiOCH with a capacitively coupled plasma using an $Ar/C_4F_8/O_2 = 80/15/5$ gas mixture at 40 mTorr.[20,35] The end result includes a CF_x polymer layer, approximately 1.5 nm thick, on the etched SiOCH surface, as shown in Fig. 4(a). The trench profile following 850 s of treatment by the Ar/O_2 plasma is shown in Fig. 4(b) where the PR mask is totally removed, exposing the top flat surface of the SiOCH. The polymer is also essentially fully removed, with small isolated islands of CF_x remaining at locations that have poor view-angles to the plasma. Damage in these profiles is interpreted primarily as the removal of $–CH_3$ (demethylation) and to a secondary degree by the formation of SiO_2^*. In this Monte Carlo based model, the removal of $–CH_3$ from the inside of pores results in the appearance of an increase in the pore size, as a layer of molecules has been removed from the surface of the pore. In reality, there is likely a collapse of the pores, a process that is not resolved in these simulations.

We found that demethylation (removal of $–CH_3$ groups from $–SiO_2–CH_3$ in porous SiOCH) is a diffusion dominated process, as suggested by Goldman *et al.*[8] The maximum depth of demethylation increases nearly linearly with time at short times and scales with $t^{1/2}$ at longer times, as shown in Fig. 4(c).[8] Pores that are open or line-of-sight to the plasma

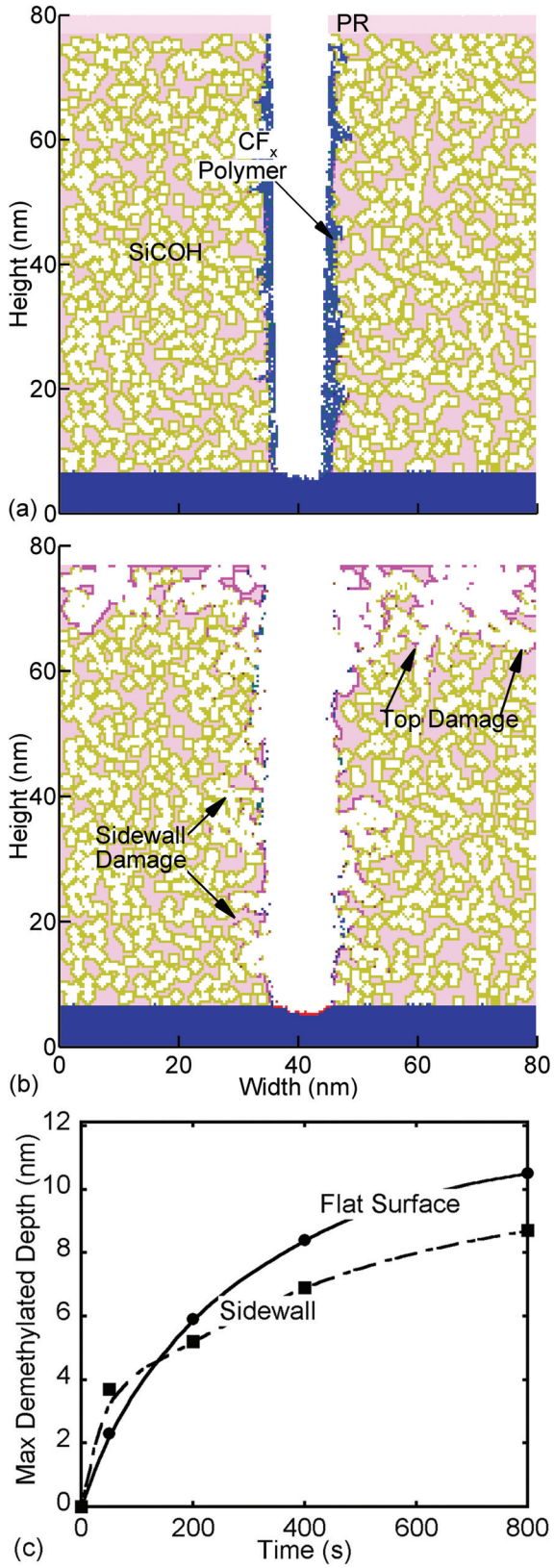

FIG. 4. (Color) Properties of plasma etched and cleaned porous SiOCH. (a) After fluorocarbon plasma etching leaving a CF_x polymer. (b) After cleaning the fluorocarbon polymer with an Ar/O_2 plasma. (c) Progression of demethylation depth in the sidewalls and on the top surface with time. [Color coding: light pink—SiO_2; olive—CH_3; light blue—CF_x; bright pink—cleaved SiO_2^*; green—$\bullet CH_{3a}$ sites after Si–C scission; brown—Si bonded CH_x ($x < 3$) groups.]

have their $-CH_3$ groups more rapidly removed by photons, ions, and O radicals. Interconnected pores deeper into the material are demethylated only after diffusion of O atoms through the porous network and, if near the surface, catalyzed by VUV bond scission.

VUV photons have a finite penetration depth into solid SiO_2. Photons that are absorbed by $-Si-CH_3$ likely produce Si–C bond scission, which then produces free radical sites, –Si•, and bond cleaved and surface trapped $\bullet CH_{3a}$. These sites speed the demethylation process. Bond cleaved $\bullet CH_{3a}$ can be etched by O as CO and H_2O, and can be removed by H radicals as CH_4. In these situations, even O_2 can promote such demethylation once the Si–C bond has been broken and $\bullet CH_{3a}$ produced.[23] One of the products of O-atom reactions with $-SiO_2-CH_3$ and $\bullet CH_{3a}$ is OH, which can itself react with SiOCH, which tends to perpetuate the demethylation process.[27]

For both Ar/O_2 and He/H_2 plasmas photon fluxes increase with power as shown in Fig. 5. The VUV photon fluxes from Ar/O_2 plasmas are 10–100 times smaller than for comparably powered He/H_2 plasmas. To decouple heavy particle kinetics and photon fluxes in the assessment of demethylation we held the heavy particle fluxes constant at their base case values and varied the fluxes of VUV photons. As the photon fluxes increase, so does the demethylation depth, shown in Fig. 5(c) for a treatment time of 900 s. Since O atoms are exothermically reactive with SiOCH there is significant demethylation even in the absence of VUV fluxes for Ar/O_2 plasmas. For He/H_2 plasmas, there is little demethylation in the absence of VUV fluxes. In both cases, increasing the VUV fluxes increases the amount of bond scission of $-SiO_2-CH_3$ (producing either $\bullet CH_{3a}$ or $-SiO_2-CH_2\bullet$), which speeds demethylation. The demethylation depth increases linearly with photon flux up to about $10^{14}\,cm^{-2}\,s^{-1}$ and then increases with $flux^{1/2}$ for the range 10^{14}–$10^{15}\,cm^{-2}\,s^{-1}$. This dependence is similar to diffusion limited damage.[8,24] The demethylation depth increases to nearly 30 nm in the Ar/O_2 plasma with increasing photon flux for fixed exposure time (or increasing fluence) and up to 11 nm in the He/H_2 plasma.

To compare the impact of VUV photons on damage of the SiOCH, the top layer of SiOCH is shown in Fig. 6 for Ar/O_2 plasma cleaning and in Fig. 7 for He/H_2 plasma cleaning without photons and with increasing photon fluxes. The demethylation is represented by the depth of removal of (olive colored) $-CH_3$ groups after plasma treatment. The change in color from pink (SiO_2) to purple represents the formation of SiO_2^*, the free radical state of SiO_2 due to Si–O bond breaking by photons. Although SiO_2^* can be etched in plasmas containing Cl and F radicals, radicals produced in Ar/O_2 or He/H_2 plasmas generally do not react with SiO_2^* as etchants, though these plasmas may passivate the free radical site.[29,31] As Worsely *et al.* suggested, Ar/O_2 plasmas can remove the entire carbon content from SiOCH but do not remove SiO_2 and leave an SiO_2-like layer.[29] On the other hand, He/H_2 plasmas less aggressively remove carbon but leave SiO_2 primarily unaffected with only some H incorporation.

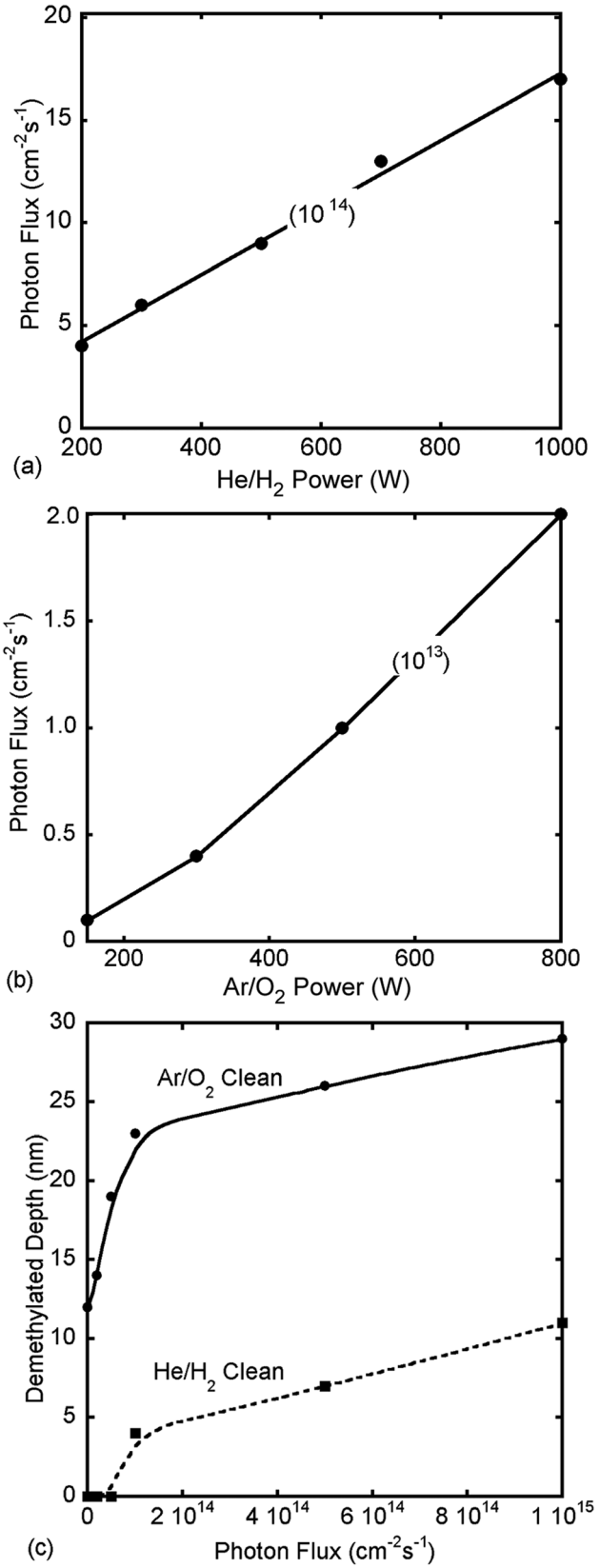

FIG. 5. Photon flux and demethylation depth properties. VUV photon flux as a function of ICP power in (a) He/H_2 and (b) Ar/O_2 plasmas. (c) Damage depth in SiOCH as a function of photon flux. The damage depth is initially linear with photon flux but later the rate of damage decreases as most of the $Si-CH_3$ sites within the absorption depth of the photons have undergone scission.

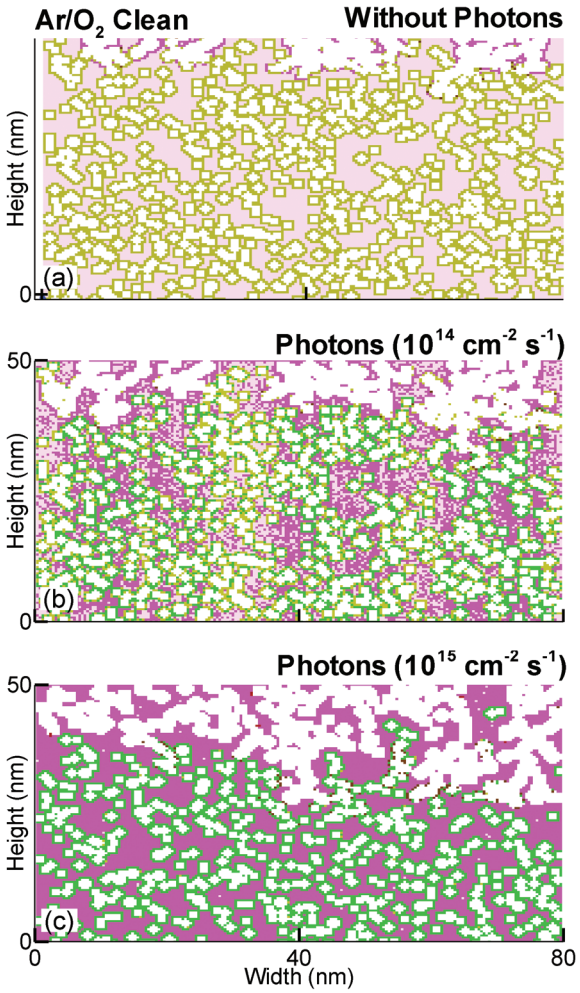

FIG. 6. (Color) SiOCH profiles showing the impact of VUV photon fluxes on demethylation during Ar/O_2 cleaning. (a) Without photons. (b) With a photon flux of $10^{14}\,cm^{-2}\,s^{-1}$, and (c) with a photon flux of $10^{15}\,cm^{-2}\,s^{-1}$. Penetration of 130 nm photons in Ar/O_2 plasmas is about 100 nm and accelerates demethylation depth to at least this depth. [Color coding: light pink—SiO_2; olive—CH_3; light blue—CF_x; bright pink—cleaved SiO_2^*; green—$\bullet CH_{3a}$ sites after Si–C scission; brown—Si bonded CH_x ($x < 3$) groups.]

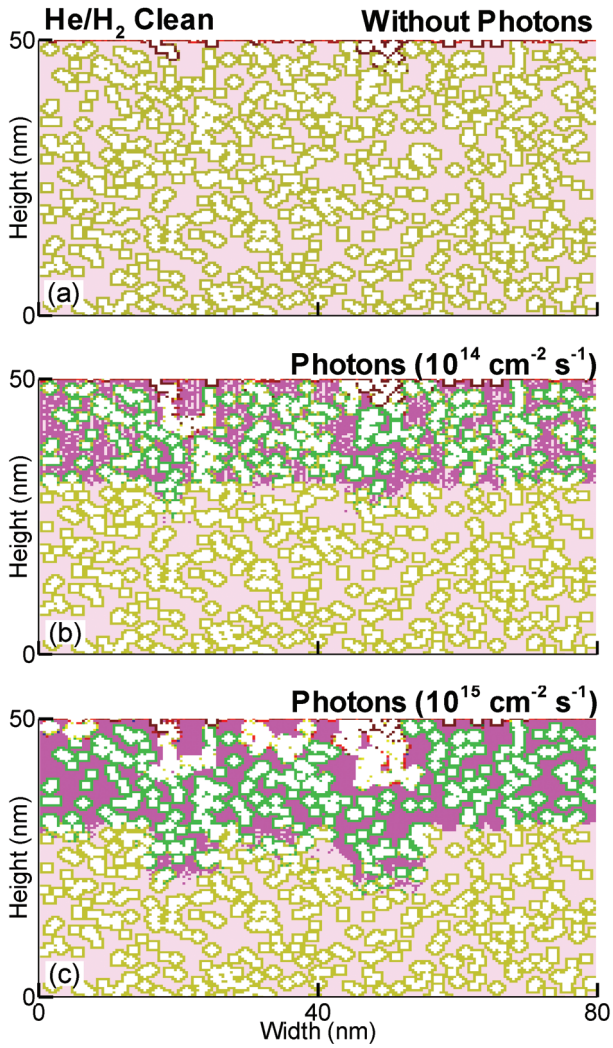

FIG. 7. (Color) SiOCH profiles showing the impact of VUV photon fluxes on demethylation during He/H_2 cleaning. (a) Without photons and with a photon flux of (b) $10^{14}\,cm^{-2}\,s^{-1}$ and (c) $10^{15}\,cm^{-2}\,s^{-1}$. Penetration of 58 nm photons in He/H_2 plasmas is about 20–30 nm and accelerates demethylation depth to at least this depth. [Color coding: light pink—SiO_2; olive—CH_3; light blue—CF_x; bright pink—cleaved SiO_2^*; green—$\bullet CH_{3a}$ sites after Si–C scission; brown—Si bonded CH_x ($x < 3$) groups.]

Increasing VUV fluxes increases the depth of demethylation and also increases the proportion of SiO_2^* sites. Although many of these free radical sites likely reconnect to reform SiO_2 without long term damage to the SiOCH, some fraction of SiO_2^* also likely remains in the long term, making the SiOCH more sensitive to damage in other processing steps. Note that in those regions of the SiOCH where, statistically, there are more pores and so more damage, the VUV penetration depth is greater. This is due to there being more line-of-sight pathways for the photons to penetrate or there being smaller line averaged mass density.

The demethylation depth is larger for flat surfaces than for the sidewalls, as shown in Fig. 4. This is due, in part, to the additional role that directional ions and photons play in the demethylation process. Due to their either line-of-sight reactivity or anisotropic trajectories, ions and photons make larger contributions to demethylation to horizontal surfaces than vertical surfaces. The average angle of incidence of ions and photons is more normal on the flat surfaces, and so the penetration is deeper perpendicular to the surface. Finally, there is also a time-lag issue. Additional time is required by O atoms, the dominant demethylation agent, to statistically enter into pores at the bottom of the trench where their fluxes are smaller than on the top surfaces, which may result in a reduced demethylation deeper in the trench.

As the interconnectivity of the SiOCH increases, there are, on average, longer average pathways from the surface for the diffusion of plasma-produced species into the SiOCH. This ultimately produces more damage (demethylation) in the porous material compared to a smaller interconnectivity.[8] For example, demethylation depth as a function of interconnectivity during Ar/O_2 and He/H_2 plasma cleaning is shown in Fig. 8 after 900 s of treatment. For both without and with photons, demethylation depth increases nearly linearly with interconnectivity. The increase in interconnectivity for a given porosity increases the likelihood of having

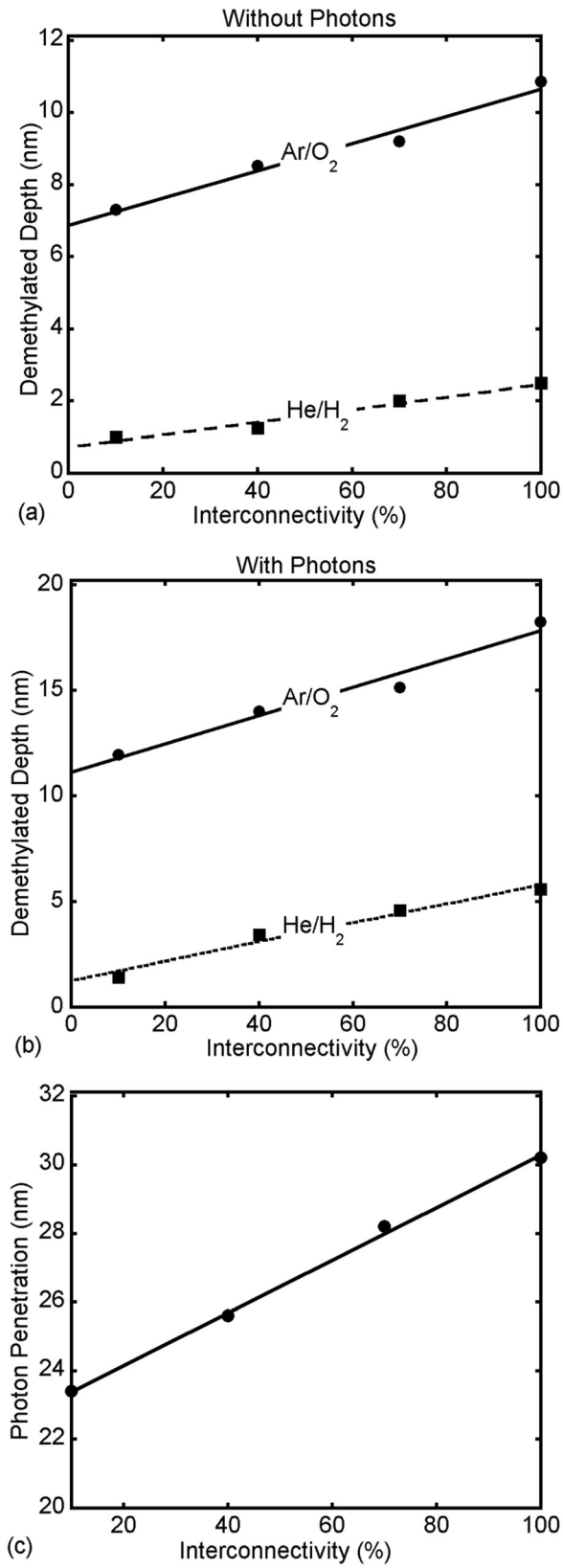

FIG. 8. Demethylation depth as a function of interconnectivity. Results are shown for Ar/O_2 and He/H_2 plasma cleaning, (a) without photons and (b) with photons for an interconnectivity range of 10%–100%. (c) Penetration depth of 58.4 nm photons from He/H_2 plasmas. Interconnected pores provide more pathways for radicals to diffuse into the SiOCH and facilitate deeper penetration of photons which produce more $Si–CH_3$ bond scission that speeds the demethylation process.

a line-of-site path through the porosity from the plasma. Even though photon penetration, on average, should depend only on porosity (or the average mass density), statistically, increasing porosity does increase the likelihood of having pores aligned that enable deeper photon penetration. We did find that the maximum photon penetration depth increases with interconnectivity, as shown in Fig. 8(c). The deeper photon penetration then facilitates greater rates of demethylation deeper into the SiOCH. As a result, damage is more sensitive to interconnectivity when including photon fluxes. Since a reasonably large porosity (~20%–30%) is required to achieve the desired low k-value, minimizing interconnectivity can be helpful in minimizing damage.[8]

SiOCH profiles for interconnectivities of 10%, 40%, and 100% following treatment with Ar/O_2 and He/H_2 plasmas are shown in Figs. 9 and 10. (The penetration depth of photons is shown by the change in color: brown $–CH_3$ groups turn green after photon produced Si–C bond scission, and light pink SiO_2 turns dark pink to represent SiO_2^*). During He/H_2 plasma cleaning, reactive H atoms also diffuse inside the material through interconnected pathways. Although H

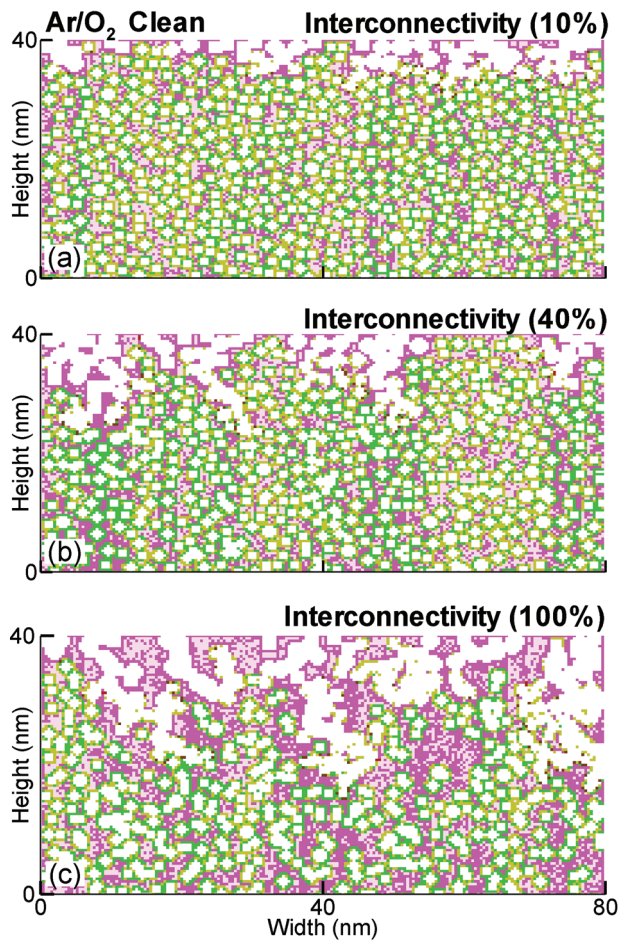

FIG. 9. (Color) Profiles showing the effects of interconnectivity on demethylation during Ar/O_2 cleaning for interconnectivities of (a) 10%, (b) 40%, and (c) 100%. Demethylated depth increases almost linearly with interconnectivity. [Color coding: light pink—SiO_2; olive—CH_3; light blue—CF_x; bright pink—cleaved SiO_2^*; green—$\bullet CH_{3a}$ sites after Si–C scission; brown—Si bonded CH_x ($x < 3$) groups.]

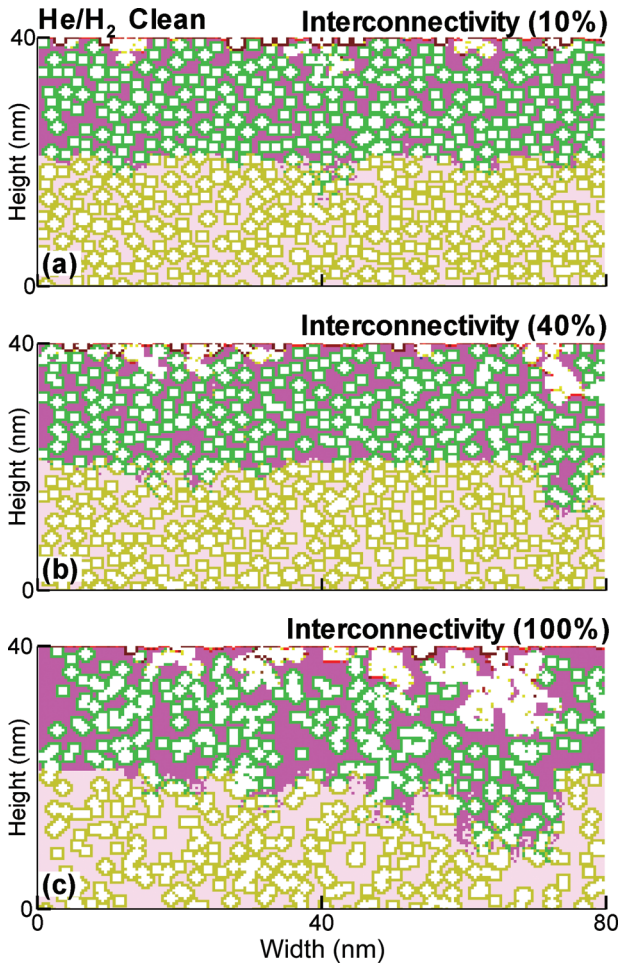

FIG. 10. (Color) Profiles showing interconnectivity effects on demethylation during He/H_2 cleaning for interconnectivities of (a) 10%, (b) 40%, and (c) 100%. Damage depth increases almost linearly with interconnectivity as for Ar/O_2 plasma cleaning. (Color coding: light pink—SiO_2; olive—CH_3; light blue—CF_x; bright pink—cleaved SiO_2^*; green—$\bullet CH_{3a}$ sites after Si–C scission; brown—Si bonded CH_x ($x < 3$) groups.]

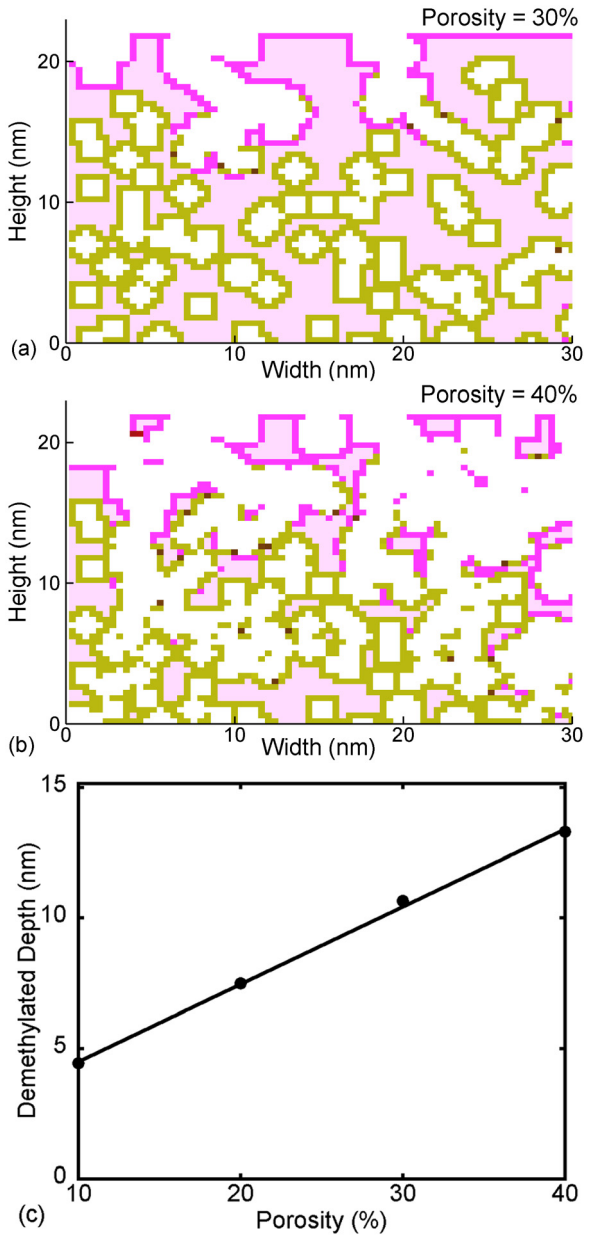

FIG. 11. (Color online) Effects of porosity on damage of SiOCH. Profiles showing damage after 900 s of Ar/O_2 plasma treatment without photons porosities of (a) 30% and (b) 40% porosity. (c) Demethylation depth as a function of porosity. The damage depth increases linearly with porosity. [Color coding: light pink—SiO_2; olive—CH_3; light blue—CF_x; bright pink—cleaved SiO_2^*; green—$\bullet CH_{3a}$ sites after Si–C scission; brown—Si bonded CH_x ($x < 3$) groups.]

atoms being lighter than O atoms can diffuse more rapidly and so possibly deeper into the SiOCH, reactions of H atoms with SiOCH are slower and produce less volatile and reactive products than reactions with O atoms.[12,29] So for otherwise identical conditions, diffusion of O atoms through interconnected pores will produce more damage than diffusion of H atoms.

The demethylation process is facilitated by Si–C bond scission by VUV photons. In Ar/O_2 plasmas, demethylation by O atoms is an exothermic process. As a result, demethylation is enhanced, though not dependent on bond scission by VUV photons. The profile of demethylation is therefore more diffusive, a consequence of O atoms' diffusion into the pores. In He/H_2 plasmas, Si–C bond scission significantly enhances the rate of demethylation, and so its depth is more closely correlated to that of the photon penetration. As a result, the demethylation depths as a function of interconnectivity in He/H_2 plasma are approximately 3 times smaller than in Ar/O_2 plasmas.

Increasing porosity increases the depth of damage in SiOCH as shown in Fig. 11 for porosities of 30% and 40% in Ar/O_2 plasmas. We found that the depth of damage increases nearly linearly with porosity as shown in Fig. 11(c).[1,29] At first glance, a more porous network should enable more rapid diffusion of radicals throughout the volume of the SiOCH and so increase the likelihood of damage at a deeper site. There is a secondary effect of photon transport—the less dense the SiOCH due to increasing porosity, the longer the penetration depth of photons due to the lower mass density of the material. These results are not independent of interconnectivity.

V. CONSEQUENCES OF VUV PHOTON FLUXES

VUV photons from Ar/O_2 and He/H_2 plasmas penetrating into SiOCH produce Si–C bond scission, which generates $\bullet CH_{3a}$ radicals on the surface of pores. These photons also produce SiO_2^* through Si–O bond cleavage.[23–25] These Si–C bond cleaved $\bullet CH_{3a}$ groups are thought to remain as a trapped surface species.[23] Since the $\bullet CH_{3a}$ groups are no longer classically chemisorbed, they are vulnerable to rapid reaction with O, O_2, or H to produce volatile CO, CO_2, or CH_4 to complete the $–CH_3$ removal process. Molecular oxygen is unable to etch $–CH_3$ when bonded to Si; however, after Si–C bond cleavage, $\bullet CH_{3a}$ is etchable by O_2, ultimately producing CO and H_2O.[23] Fluxes of VUV photons from the plasma can therefore significantly increase the rate of demethylation compared to fluxes of only O or H atoms. The 130 nm photons from O atoms in Ar/O_2 plasmas have a penetration depth of ≈100 nm into SiOCH and so can increase demethylation to at least this depth provided the interconnectivity enables penetration of plasma-produced radicals into the network.[23,25] The 58 nm photons produced by He* in He/H_2 plasmas have penetration depths of only ~20 nm, and are energetic enough to break both Si–O and Si–C bonds.[24] Due to the less reactive nature of H radicals with $–SiO_2–CH_x$ groups, Si–C bond cleavage by photons from He/H_2 plasmas is a more important precursor to the removal of hydrophobic $–CH_3$ groups by H atoms than oxygen containing plasmas where the carbon removal step is exothermic.[25]

The depths of demethylation shown in Figs. 6 and 7 as a function of photon flux are consistent with experimentally measured ranges of damage of SiOCH for photon fluxes of 10^{14}–10^{15} cm^{-2} s^{-1}.[25] Damage of the SiOCH increases in depth as the photon fluxes increase. This is in large part due to saturation of the scission of the Si–C bonding in $–SiO_2–CH_3$. The maximum demethylation depth is to a large degree determined by the penetration depth of the particular wavelength into the SiOCH. The actual demethylation depth is then determined by the degree of $Si–CH_3$ scission within that maximum depth. In some ways, damage is a function of the fluence of photons (photons/cm^2) as opposed to simply flux (photons/cm^2 s). A longer treatment time for a given flux of photons will produce a deeper demethylation. Damage of SiOCH for the same fluence of VUV photons (keeping VUV photon flux × time = constant) is shown in Fig. 12 for He/H_2 and Ar/O_2 plasma cleans. With the same fluence, SiOCH was treated in Ar/O_2 plasmas with photon fluxes of 5×10^{14} and 10^{15} cm^{-2} s^{-1}. The amount of Si–C bond scission was essentially the same in both cases. However, O radicals had twice the time to diffuse into the network for the lower photon flux, and so produced somewhat deeper damage. Similarly, in He/H_2 plasmas for equal photon fluence, H radicals having more time to diffuse into the network caused more damage to the SiOCH with the lower photon flux.

Fluorocarbon plasma etched trenches in porous SiCOH producing CF_x polymer covered sidewalls were cleaned in Ar/O_2 and He/H_2 plasmas. The resulting profiles are shown in Fig. 13 with and without photon fluxes. During the overetch required to remove all of the CF_x polymers, O_2 containing

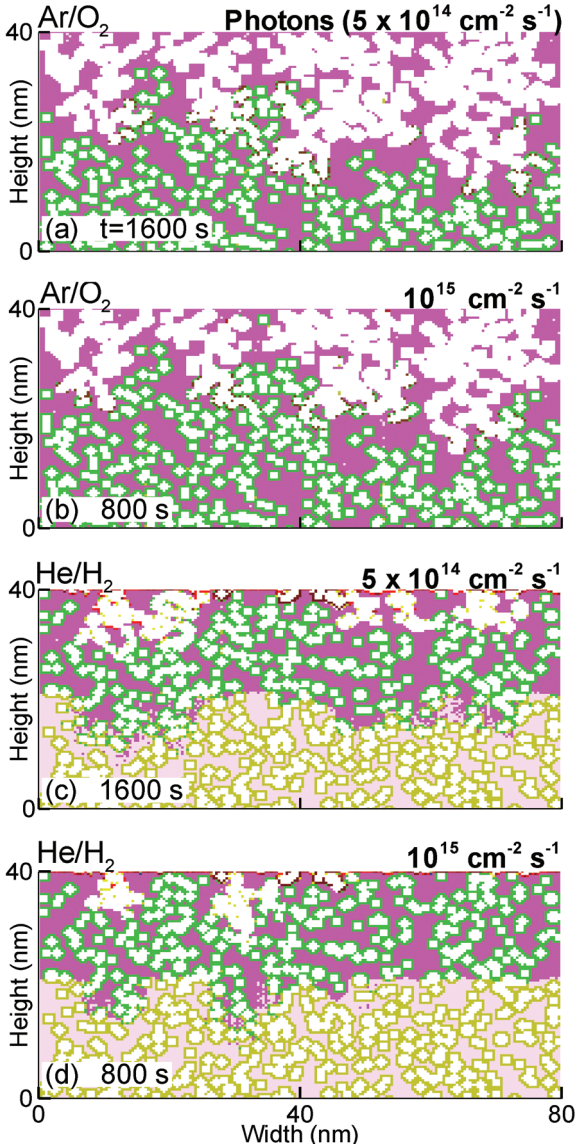

FIG. 12. (Color) SiOCH treated with different fluxes of VUV photons for the same fluence. (a) Ar/O_2 plasma clean with a 5×10^{14} cm^{-2} s^{-1} photon flux treated for 1600 s, and (b) 10^{15} cm^{-2} s^{-1} flux treated for 800 s. (c) He/H_2 plasma clean with a 5×10^{14} cm^{-2} s^{-1} photon flux treated for 1600 s, and (d) 10^{15} cm^{-2} s^{-1} flux treated for 800 s. For a constant fluence, the amount of Si–C bond scission is essentially the same, but for longer treatment times there is more opportunity for radical fluxes to diffuse into the SiOCH and so cause more damage. [Color coding: light pink—SiO_2; olive—CH_3; light blue—CF_x; bright pink—cleaved SiO_2^*; green—$\bullet CH_{3a}$ sites after Si–C scission; brown—Si bonded CH_x ($x < 3$) groups.]

plasmas caused significant demethylation by removing $–CH_3$ groups. (Damage is shown as pink sites indicating an SiO_2 site that has lost $–CH_3$.) On the other hand, H radicals remove $–CH_3$ less aggressively in large part because hot H atoms are required for efficient removal of $–CH_3$, and as H atoms diffuse into the pores, they thermalize and so lose reactivity. In the absence of VUV illumination, He/H_2 may clean porous SiCOH without causing significant damage, only modifying the surface that sees larger fluxes of hot H atoms, as suggested by others.[12,16]

However, with 58 nm photon fluxes in He/H_2 plasmas, the resulting Si–C bond scission enables damage, both on

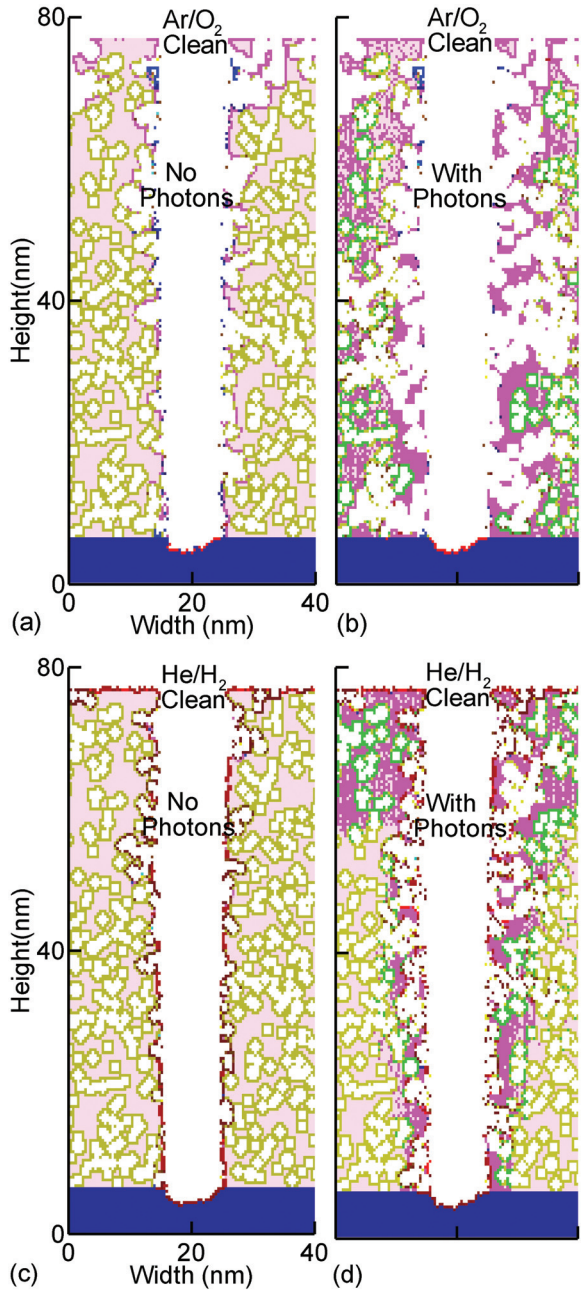

FIG. 13. (Color) Trenches in SiOCH following cleaning of CF_x polymer. Cleaning by Ar/O_2 plasmas (a) without and (b) with VUV photons. Cleaning by He/H_2 plasmas (c) without and (d) with VUV photons. Presence of photons accelerates damage by Si–C bond scission for gas mixtures. [Color coding: light pink—SiO_2; olive—CH_3; light blue—CF_x; bright pink—cleaved SiO_2^*; green—•CH_{3a} sites after Si–C scission; brown—Si bonded CH_x ($x < 3$) groups.]

the sidewalls and on the top of the feature. Due to the grazing view-angle to the plasma deep in the trench, the depth of the damaged layer due to photon absorption is smaller than on the top of the feature. As the absorption length of the photons produced in Ar/O_2 plasmas is longer than in He/H_2 plasmas, the extent of the damage perpendicular to the sidewalls is correspondingly thicker. During He/H_2 plasma cleaning, Si–C bond scission that causes the removal of $–CH_3$ from $Si–CH_3$ as CH_4 eventually leads to the formation of hydrophobic $–Si–H_n$, which additionally protects the Si from moisture adsorption.[29]

VI. COMPARISON OF TRENDS WITH PRIOR WORKS

As reported by Goldman *et al.*[8] and Vanstreels and Urbanowicz,[16] we found that diffusion of O atoms is the dominant process for producing damage by Ar/O_2 plasmas in porous SiOCH. We also found that, as suggested by Jinnai *et al.*[25] and Lee and Graves,[23] scission of Si–C bonds by VUV fluxes can increase the rate of damage. We found that in the absence of VUV fluxes, He/H_2 plasmas modify the low-*k* surface but do not efficiently remove C atoms, which agrees with reports that found little damage in SiOCH after processing in a downstream He/H_2 plasma reactor where the flux of VUV photons is negligible.[12,16] However, the 58 nm photons produced in He/H_2 plasmas can cause Si–C bond scission and so likely act as a precursor to damage, as concluded by Jinnai *et al.*[25] We found that the depth of damage ($–CH_3$ removal) for Ar/O_2 plasma treatment when treated for the same duration is approximately 3 times larger than He/H_2 plasma cleaning. These results align with those reported by Worsley *et al.*,[29] albeit for plasma damage produced in a capacitively coupled system. They found deeper damage of SiOCH in Ar/O_2 mixtures compared to Ar/H_2 mixtures but deeper nondamaging modification in Ar/H_2 mixtures, perhaps due to the higher mobility of H atoms in the SiOCH. They also found etch rates and the rate of carbon removal were significantly higher in the Ar/O_2 plasmas due to the highly reactive O-atom fluxes. Based on the ΔH of the reaction, Worsely *et al.* estimated that CH_3 removal by O atoms is more than 2 times energetically favorable compared to removal by H atoms.[29]

Possemme *et al.*[36] investigated the carbon depletion and increase in *k-value* of SiOCH having a low 8% porosity (lp-SiOCH) and a high 45% porosity (hp-SiOCH). Plasma ashing experiments were performed in downstream plasma (DSP) reactors using H_2/Ar, H_2/He, H_2/N_2, O_2, and O_2/N_2 plasmas where ion bombardment and photon illumination are not important. For the lp-SiOCH, carbon depletion was small in the absence of H_2 or O_2 in the plasma. The greatest carbon depletion was about 10% with O_2 in the DSP. For the hp-SiOCH, carbon depletion increased to about 35% with O_2 containing DSP. The depletion with H_2/N_2 was about 1/3 that of the O_2 containing plasmas. These trends align with those predicted here—more porous materials subject to oxygen radical containing fluxes being more susceptible to carbon removal than low porosity materials subject to hydrogen atom containing fluxes.

To avert the potentially damaging effects of O_2 based plasma cleaning and resist stripping of SiOCH, the use of H_2 based plasmas has been considered as an attractive option.[37] Although pure H_2 plasmas can significantly minimize damage, the rate of removal of PR is relatively slow.[38] Increasing substrate temperature to increase the rate of PR removal is an option; however, the increase in temperature also increases the rate of carbon removal.[39] To speed the rate of

PR removal, N_2 or Ar can be mixed with H_2. However, the increase in removal rate is small.[38,39] As a result, alternative chemistries are also being investigated for plasma ashing of PR, among them being the use of CO_2, which produces plasmas capable of stripping PR at acceptable rates while not appreciably damaging the low-k material.[40] CO_2 (or CO) based plasmas have been reported to produce a significantly thinner damage layer compared to O_2 plasmas when removing the same thickness of PR.[37] Although O radicals are the primary agent for PR stripping in both CO_2 and O_2 based plasmas, the lower density of O atoms in CO_2 based plasmas and perhaps some replacement of removed carbon compared to O_2 based plasmas produces less damage to the low-k material.[37] There are also system integration issues that may favor the use of CO_2 plasmas, such as being able to use the same plasma reactor for cleaning as used for the etching in fluorocarbon plasmas.[41]

VII. CONCLUDING REMARKS

We computationally investigated Ar/O_2 and He/H_2 plasma damage in porous SiOCH. While diffusion of radicals into the network is likely the primary cause for damage of porous SiOCH, the presence of photons can accelerate the rate of damage. Plasmas that can remove $–CH_3$ by virtue of exothermic reactions will cause more damage to SiOCH than plasmas that remove such groups relying on endothermic reactions, and this in large part explains the higher damage potential of Ar/O_2 plasmas compared to He/H_2 plasmas. The wavelength of photons present in the plasmas is important as the penetration depth of photons increases with wavelength in the VUV and deep UV, and energies of photons decrease with wavelength. Photons having wavelengths <140 nm have enough energy (>9 eV) to cause Si–C and Si–O bond scission and play a major role in the damage of SiOCH. The interconnectivity of the pores enables radicals to etch methyl groups deep in the SiOCH by diffusing through the network. If pores are relatively isolated (less interconnected), reactive species will not find a well-connected path to diffuse and remove $–CH_3$ groups located on deeper pore-walls. As such, SiOCH with low interconnectivity, cleaned by plasma-producing fluxes containing small fractions of O atoms, and producing photons that do not penetrate deeply into the material may be a way to maintain low-k integrity.

ACKNOWLEDGMENTS

This work was supported by the Semiconductor Research Corp. The authors acknowledge and sincerely thank Denis Shamiryan of GLOBALFOUNDRIES for his insights on the topic of this paper.

[1]M. R. Baklanov, K. P. Mogilnikov, and Q. T. Le, Microelectron. Eng. **83**, 2287 (2006).
[2]K. Maex, M. Baklanov, D. Shamiryan, F. Iacopi, S. H. Brongersma, K. Maex, and Z. S. Yanovitskaya, J. Appl. Phys. **93**, 8793 (2003).
[3]G. Mannaert, M. R. Baklanov, Q. T. Le, Y. Travaly, W. Boullart, S. Vanhaelemeersch, and A. M. Jonas, J. Vac. Sci. Technol. B **23**, 2198 (2005).
[4]H. Seo, S. B. Kim, J. Song, Y. Kim, H. Soh, Y. C. Kim, and H. Jeon, J. Vac. Sci. Technol. B **20**, 1548 (2002).
[5]K. Sakuma, K. Machida, K. Kamoshida, Y. Sato, K. Imai, and E. Arai, J. Vac. Sci. Technol. B **13**, 902 (1995).
[6]M. A. Hartney, D. W. Hess, and D. S. Soane, J. Vac. Sci. Technol. B **7**, 1 (1989).
[7]E. Kondoh, T. Asano, A. Nakashima, and M. Komatu, J. Vac. Sci. Technol. B **18**, 1276 (2000).
[8]M. A. Goldman, D. B. Graves, G. A. Antonelli, S. P. Behera, and J. A. Kelber, J. Appl. Phys. **106**, 013311 (2009).
[9]H. Shi, J. Bao, R. S. Smith, H. Huang, J. Liu, P. S. Ho, M. L. McSwiney, M. Moinpour, and G. M. Kloster, Appl. Phys. Lett. **93**, 192909 (2008).
[10]J. Proost, E. Kondoh, G. Vereecke, M. Heyns, and K. Maex, J. Vac. Sci. Technol. B **16**, 2091 (1998).
[11]J. Proost, M. Baklanov, K. Maex, and L. Delaey, J. Vac. Sci. Technol. B **18**, 303 (2000).
[12]D. Shamiryan, M. R. Baklanov, S. Vanhaelemeersch, and K. Maex, J. Vac. Sci. Technol. B **20**, 1923 (2002).
[13]M. Urbanowicz, M. R. Baklanov, J. Heijlen, Y. Travaly, and A. Cockburn, Electrochem. Solid-State Lett. **10**, G76 (2007).
[14]A. M. Urbanowicz, D. Shamiryan, A. Zaka, P. Verdonck, S. De Gendt, and M. R. Baklanov, J. Electrochem. Soc. **157**, H565 (2010).
[15]F. N. Dultsev, A. M. Urbanowicz, and M. R. Baklanov, Mater. Res. Soc. Symp. Proc. **1079**, N07-03 (2008).
[16]K. Vanstreels and A. M. Urbanowicz, J. Vac. Sci. Technol. B **28**, 173 (2010).
[17]M. J. Kushner, J. Phys. D **42**, 194013 (2009).
[18]K. Rajaraman and M. J. Kushner, J. Phys. D: Appl. Phys. **37**, 1780 (2004).
[19]J. Shoeb and M. J. Kushner, J. Vac. Sci. Technol. A **30**, 041304 (2012).
[20]A. Agarwal and M. J. Kushner, J. Vac. Sci. Technol. A **27**, 37 (2009).
[21]A. Sankaran and M. J. Kushner, J. Vac. Sci. Technol. A **22**, 1242 (2004).
[22]F. Ossler, J. Larsson, and M. Alden, Chem. Phys. Lett. **250**, 287 (1996).
[23]J. Lee and D. B. Graves, J. Phys. D **43**, 425201 (2010).
[24]J. R. Woodworth, M. E. Riley, V. A. Amatucci, T. W. Hamilton, and B. P. Aragon, J. Vac. Sci. Technol. A **19**, 45 (2001).
[25]B. Jinnai, S. Fukuda, H. Ohtake, and S. Samukawa, J. Appl. Phys. **107**, 043302 (2010).
[26]M. Chaudhari, J. Du, S. Behera, S. Manandhar, S. Gaddam, and J. Kelber, Appl. Phys. Lett. **94**, 204102 (2009).
[27]O. V. Braginsky *et al.*, J. Appl. Phys. **108**, 073303 (2010).
[28]M. F. A. M. Van Hest, A. Klaver, D. C. Schram, and M. C. M. Van De Sanden, Thin Solid Films **449**, 40 (2004).
[29]M. A. Worsley, S. F. Bent, S. M. Gates, N. C. M. Fuller, W. Volksen, M. Steen, and T. Dalton, J. Vac. Sci. Technol. B **23**, 395 (2005).
[30]K. Singh, A. A. Kumbhar, and R. O. Dusane, Mater. Lett. **60**, 1579 (2006).
[31]J. Pelletier and M. J. Cooke, J. Vac. Sci. Technol. B **7**, 59 (1989).
[32]K. Hassouni, T. A. Grotjohn, and A. Gicquel, J. Appl. Phys. **86**, 134 (1999).
[33]G. D. Billing and E. R. Fisher, J. Chem. Phys. **18**, 225 (1976).
[34]T. Kikkawa, S. Kuroki, S. Sakamoto, K. Kohmura, H. Tanaka, and N. Hata, J. Electrochem. Soc. **152**, G560 (2005).
[35]M. Wang and M. J. Kushner, J. Appl. Phys. **107**, 023309 (2010).
[36]N. Posseme, T. Chevolleau, T. David, M. Darnon, O. Louveau, and O. Joubert, J. Vac. Sci. Technol. B **25**, 1928 (2007).
[37]M.-S. Kuo, A. R. Pal, G. S. Oehrlein, P. Lazzeri, and M. Anderle, J. Vac. Sci. Technol. B **28**, 952 (2010).
[38]J. Lee, W.-J. Park, D.-H. Kim, J. Choi, K. Shin, and I. Chung, Thin Solid Films **517**, 3847 (2009).
[39]M.-S. Kuo, X. Hua, G. S. Oehrlein, A. Ali, P. Jiang, P. Lazzeri, and M. Anderle, J. Vac. Sci. Technol. B **28**, 284 (2010).
[40]G. L. Weibel and C. K. Ober, Microelectron. Eng. **65**, 145 (2003).
[41]M.-S. Kuo and G. S. Oehrlein, J. Vac. Sci. Technol. B **28**, 1104 (2010).